

Electronic Supplementary Information

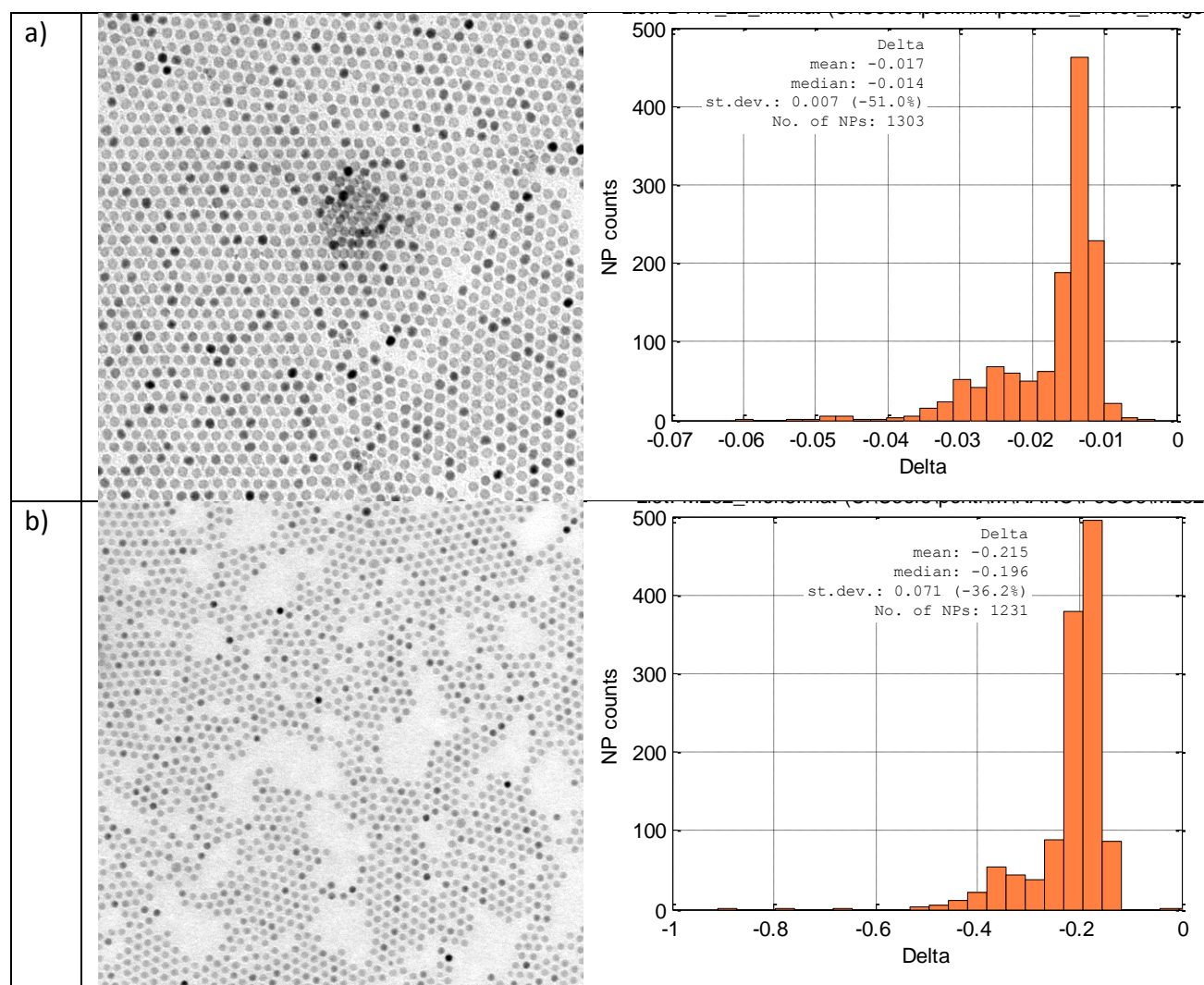
PEBBLES and PEBBLEJUGGLER: Software for Accurate, Unbiased, and Fast
Measurement and Analysis of Nanoparticle Morphology from Transmission
Electron Microscopy (TEM) Micrographs

S. Mondini^a, A. M. Ferretti^a, A. Puglisi^{a,b,§}, and A. Ponti^{a,b,*}

Fraction of NPs of inorganic compounds showing diffraction intensity significant with respect to incoherent scattering.

In addition to incoherent scattering, crystalline NPs can strongly diffract electrons when they are properly oriented even though this is not a very frequent situation for randomly oriented NPs. When aiming at measuring the size distribution from a set of several thousand randomly oriented NPs, strongly diffracting NPs (with respect to their incoherent scattering) could even be neglected from a statistical standpoint since they typically are a minority among the imaged NPs. For instance, in Fig. S1 (and in Fig. 1(d) in the main text) one can see that most NPs show similar contrast since they have similar size and scatter only incoherently, so that contrast is orientation independent. The rest of the NPs have differently darker gray shades as they have a significant contribution from diffraction scattering. The different shades of gray mirror the strength and the excitation error of the particular reflection. Indeed, even if the small size of nanocrystals makes the Bragg diffraction condition less stringent (broader diffraction spots in reciprocal space), the probability that a crystalline NP strongly diffracts is not large. From the analysis of the distribution of the image intensity (Δ), it turns out that NPs fall into three groups. The first group corresponds to a narrow peak at small Δ and comprises NPs without significant diffraction scattering and amounts at about 80% of the analyzed NPs. The second group makes up a broad peak at medium Δ and comprises NPs with significant diffraction (about 20%). The last group comprises very strongly diffracting NPs (about 1-2%) which appear as a jagged distribution tail towards more negative Δ . Such experimental distributions, though limited to iron and manganese oxides, show that most NPs in a randomly-oriented set of predominantly scatter by incoherent processes, at least in simple inorganic compounds.

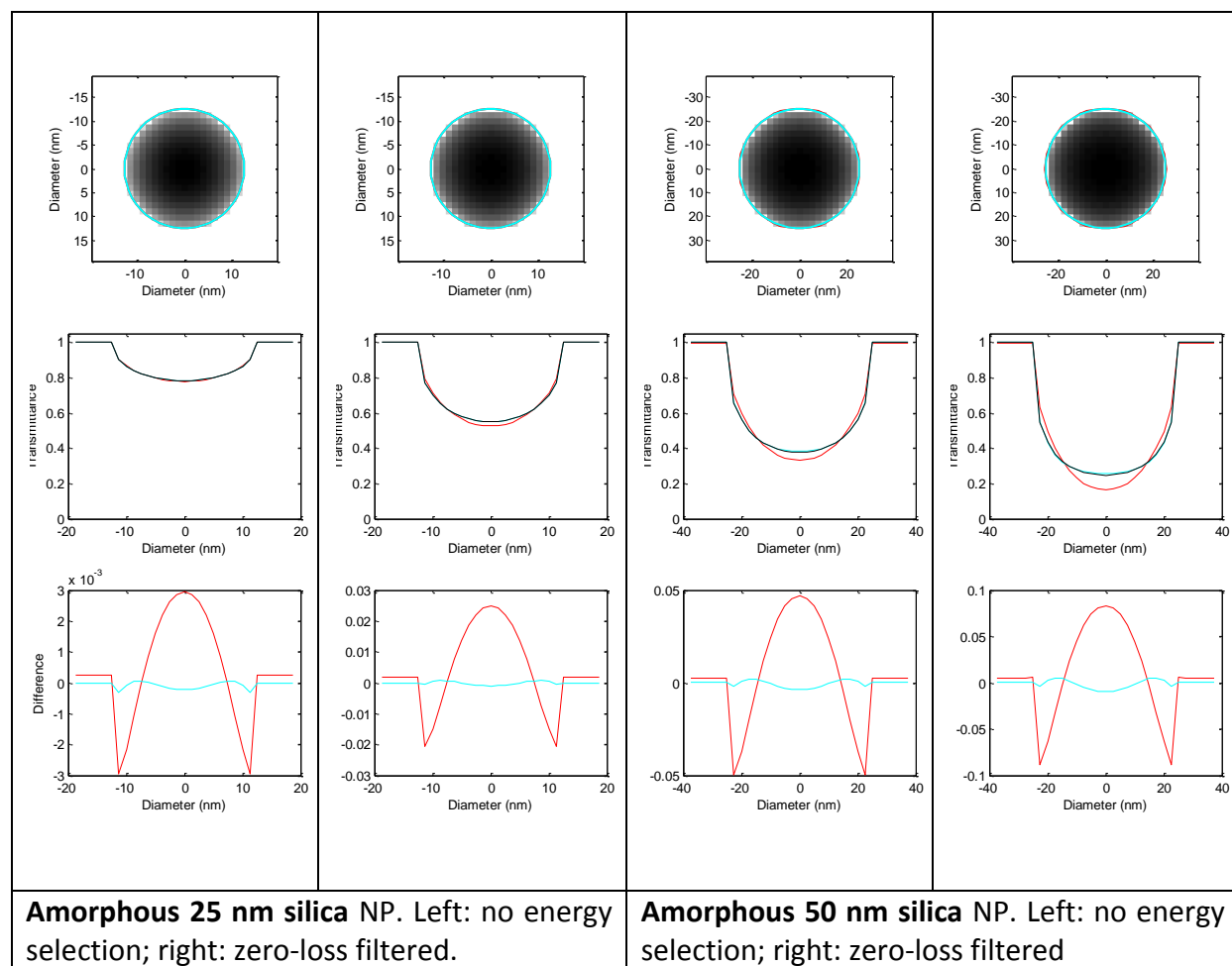
Figure S1. Images of monodisperse crystalline NPs [(a) 14 nm manganese(II) oxide, (b) 7.5 nm magnetite] showing that NPs with strong diffraction scattering are relatively rare. Left column: TEM micrograph, size: (a) 615 x 615 nm, (b) 470 x 470 nm. Right column: histogram of the distribution of the NP image intensity Δ corresponding to each image.

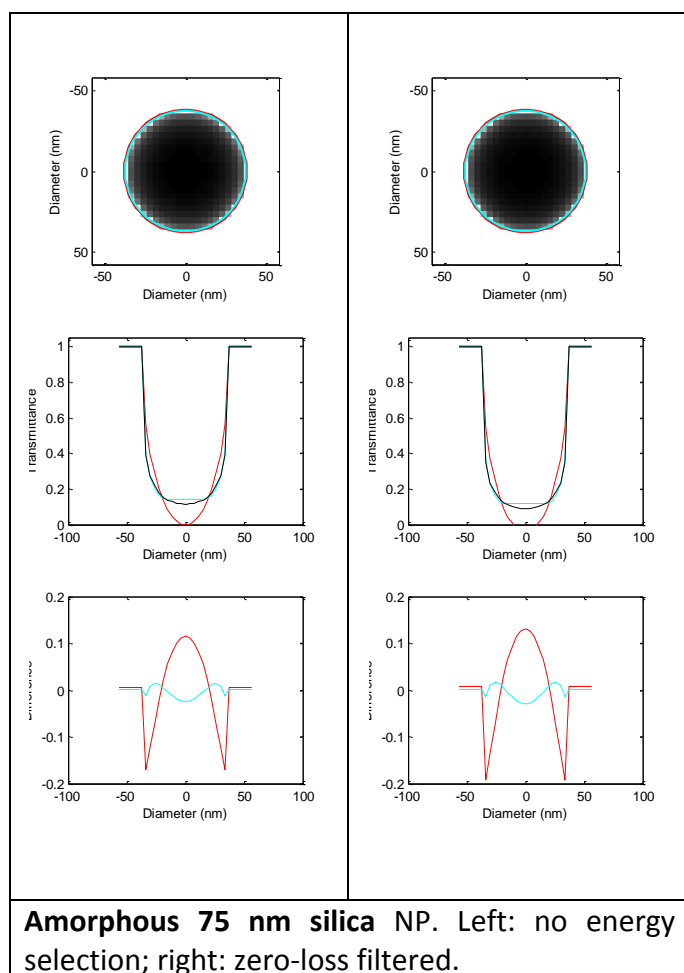


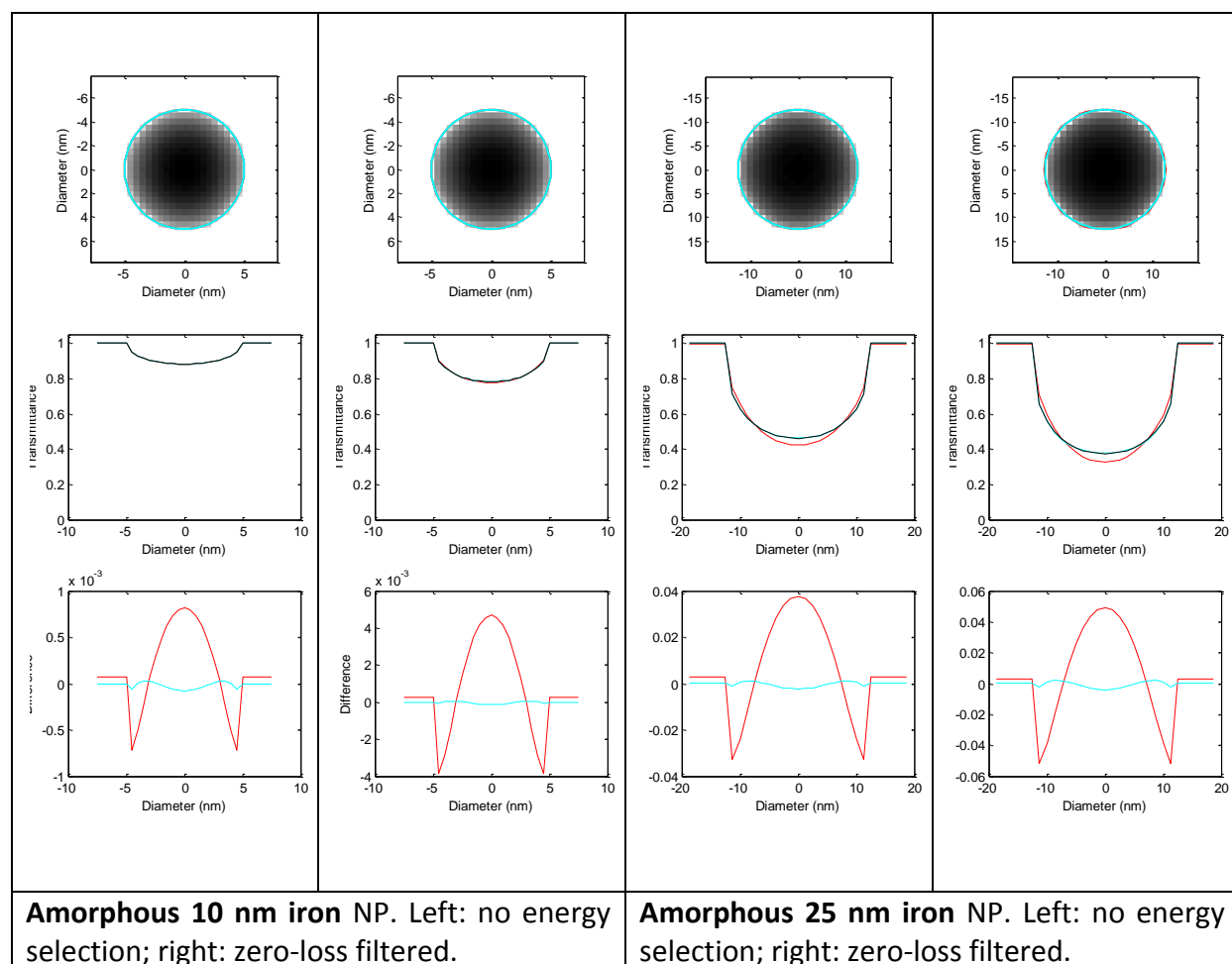
Anyway, fitting of diffracting NP is available in PEBBLES so that (i) there is no need to expunge diffracting NPs from the fitting procedure when applied to an entire TEM micrograph, and (ii) PEBBLES can also be used to analyze dark-field images which are dominated by diffraction contrast.

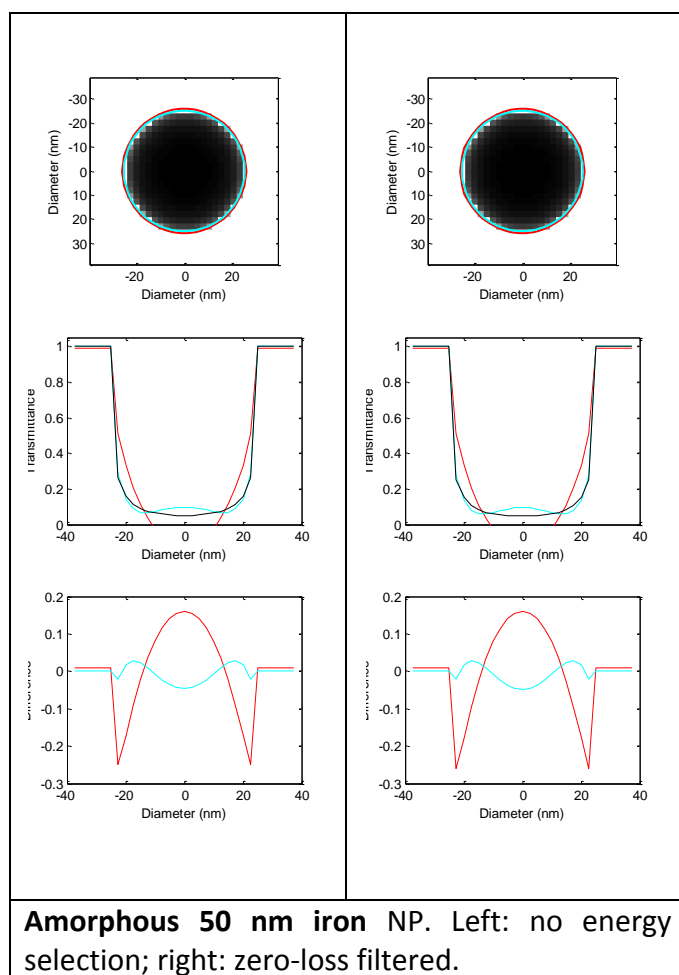
Accuracy testing of the intensity models using simulated reference images

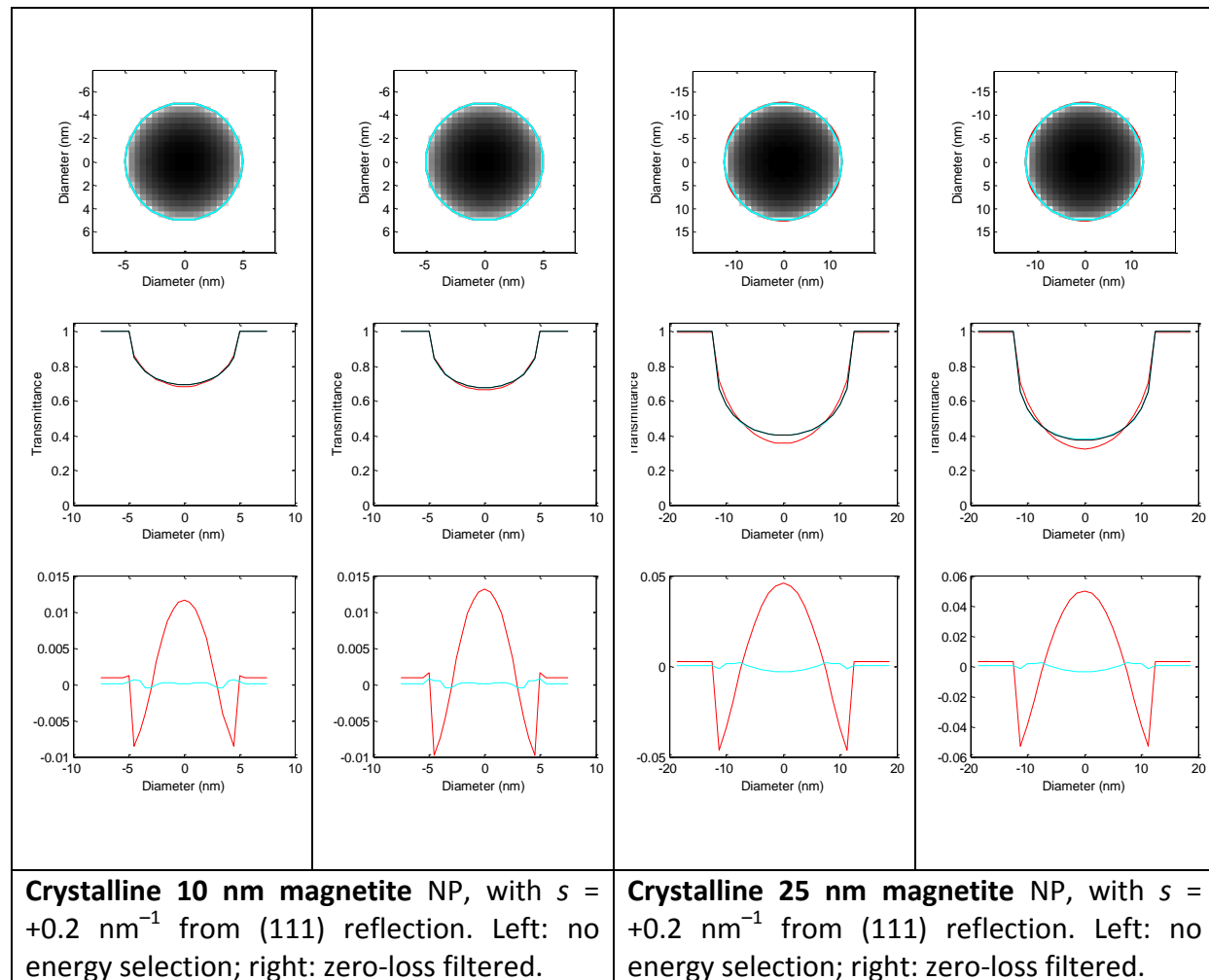
Figure S2. Results of fitting a linear $J = j_0 + j_1 t$ or quadratic $J = j_0 + j_1 t + j_2 t^2$ model to reference images of amorphous silica (SiO_2) and gold (Au) and crystalline magnetite (Fe_3O_4) and fcc gold (Au) spherical NPs computed by general theory including elastic and inelastic incoherent scattering, using electrons accelerated to $E_0 = 200$ keV and an objective lens aperture with collection angle $\beta = 5$ mrad. All reference images are dominated by incoherent scattering as the crystalline NPs are mis-oriented ($s = 0.2 \text{ nm}^{-1}$) from the strong (111) reflection. Images either with or without zero-loss-filtering are shown. Black lines: reference image; red lines: linear model; cyan lines: quadratic model. Top row: gray-scale view of the simulated image with edges of the fitted NPs; comparison of the reference and fitted NP profiles; bottom row: difference between reference and fitted profiles.

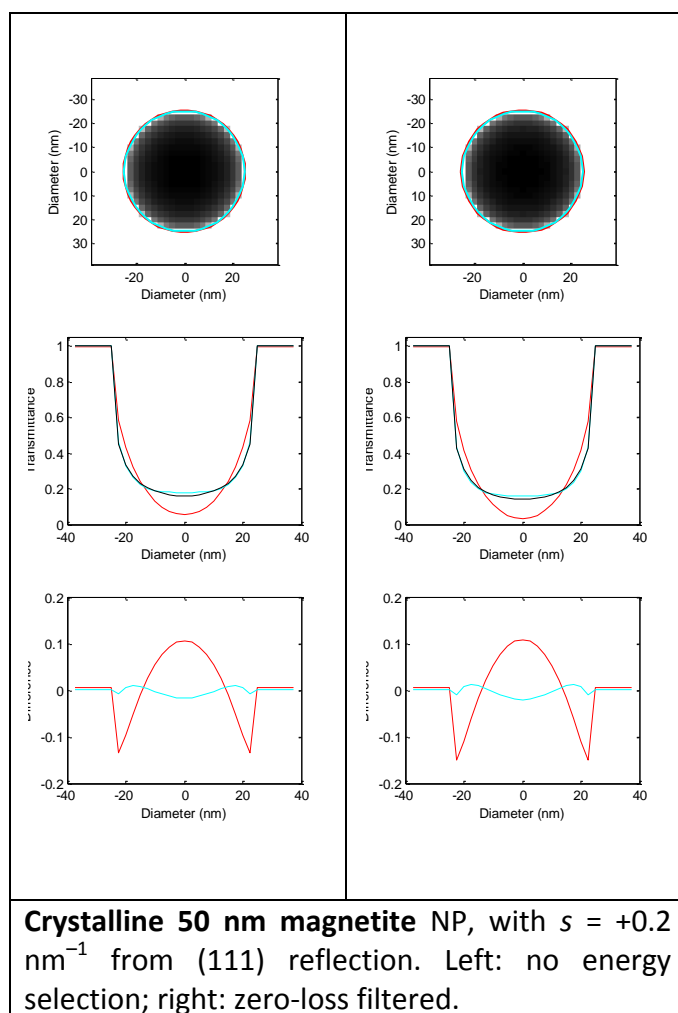


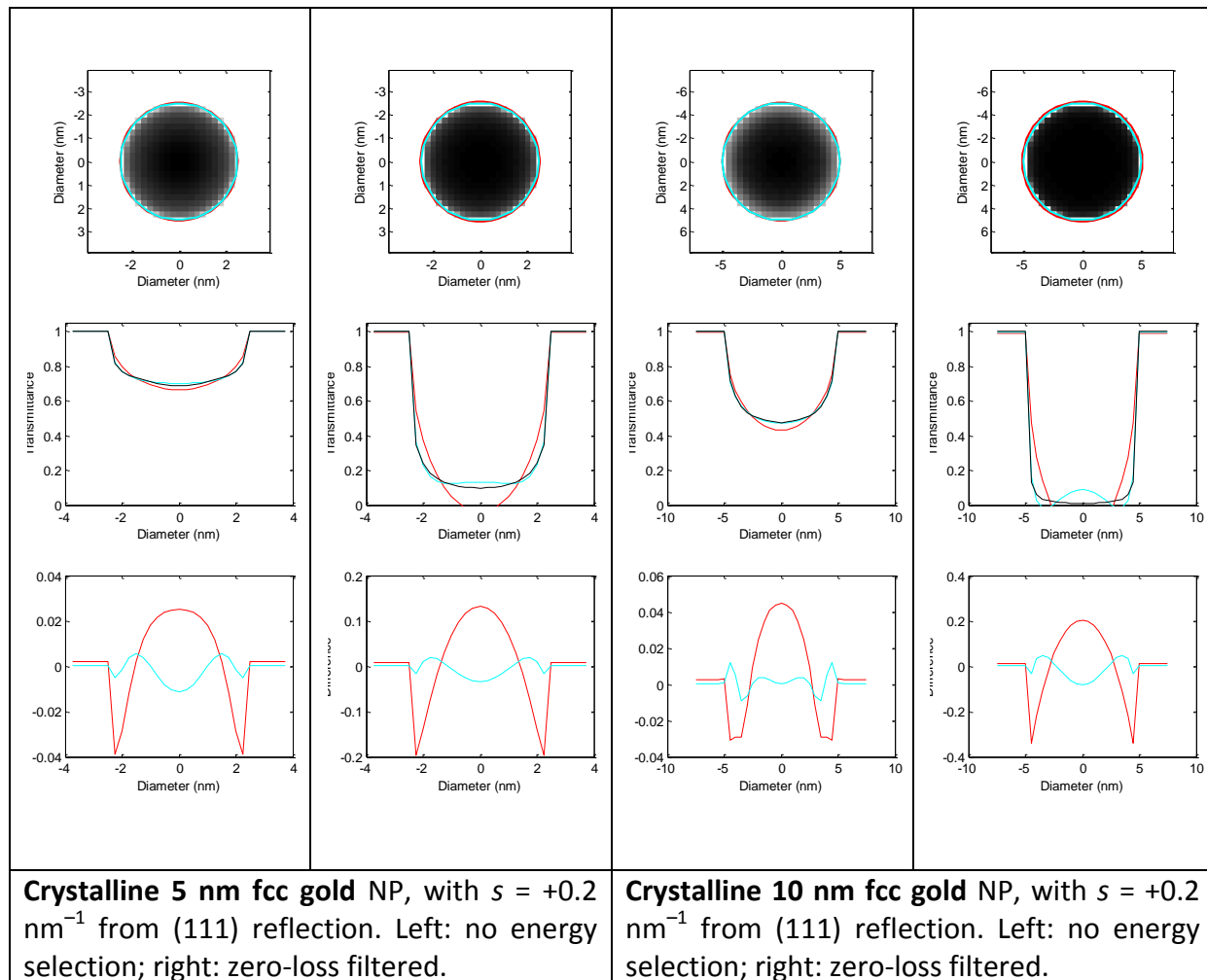












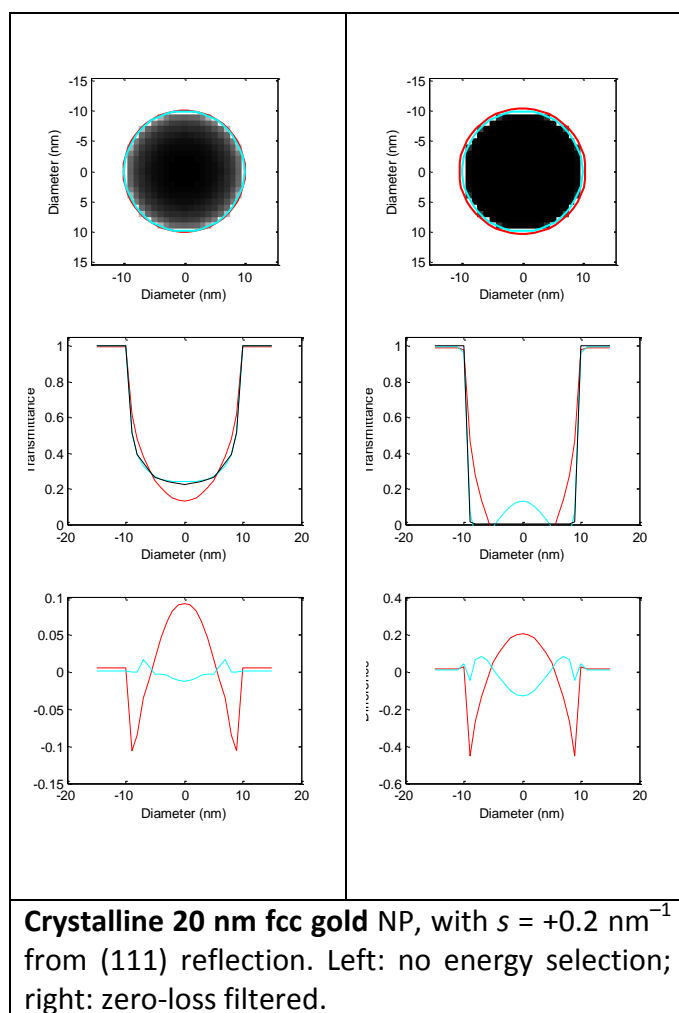
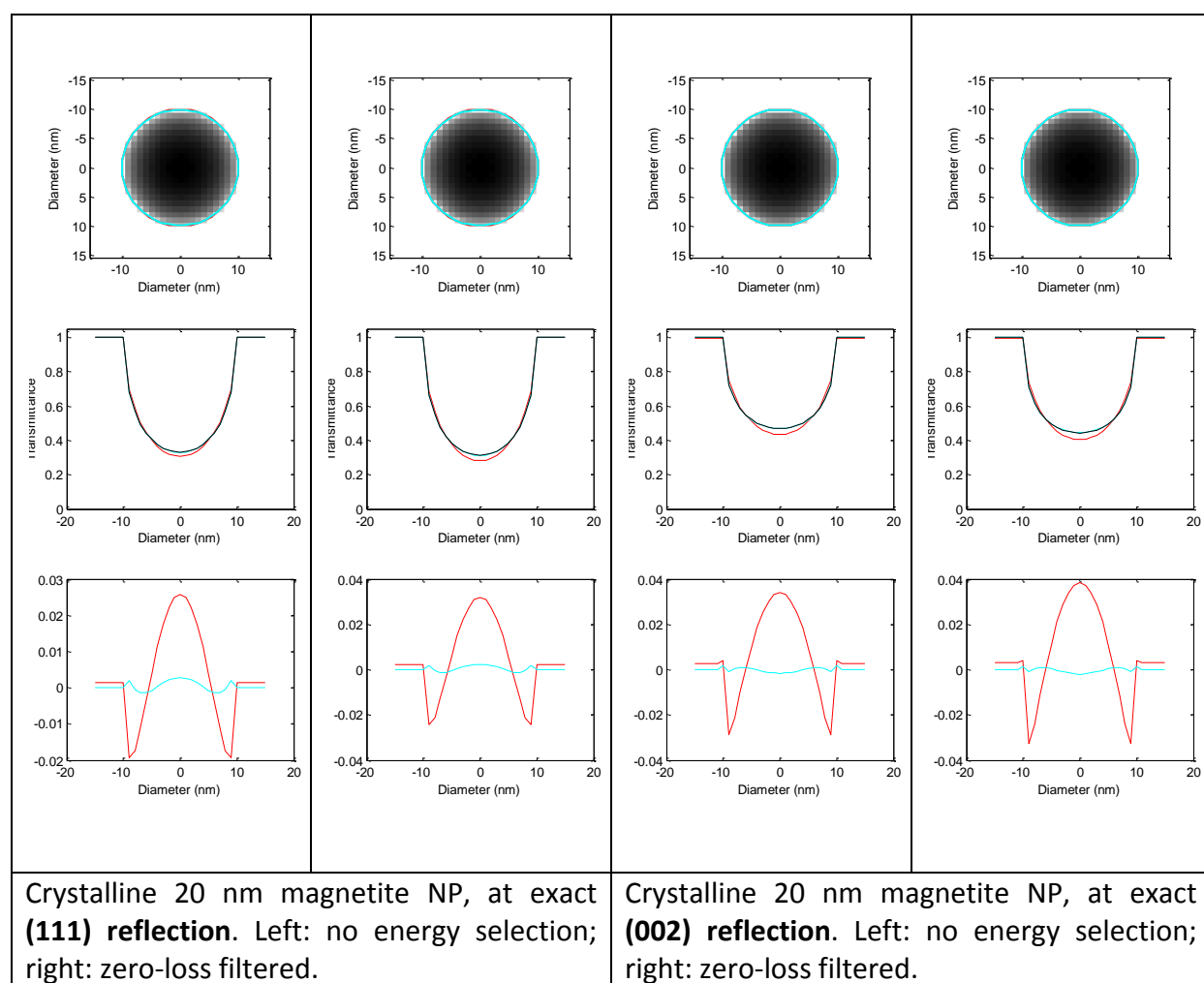
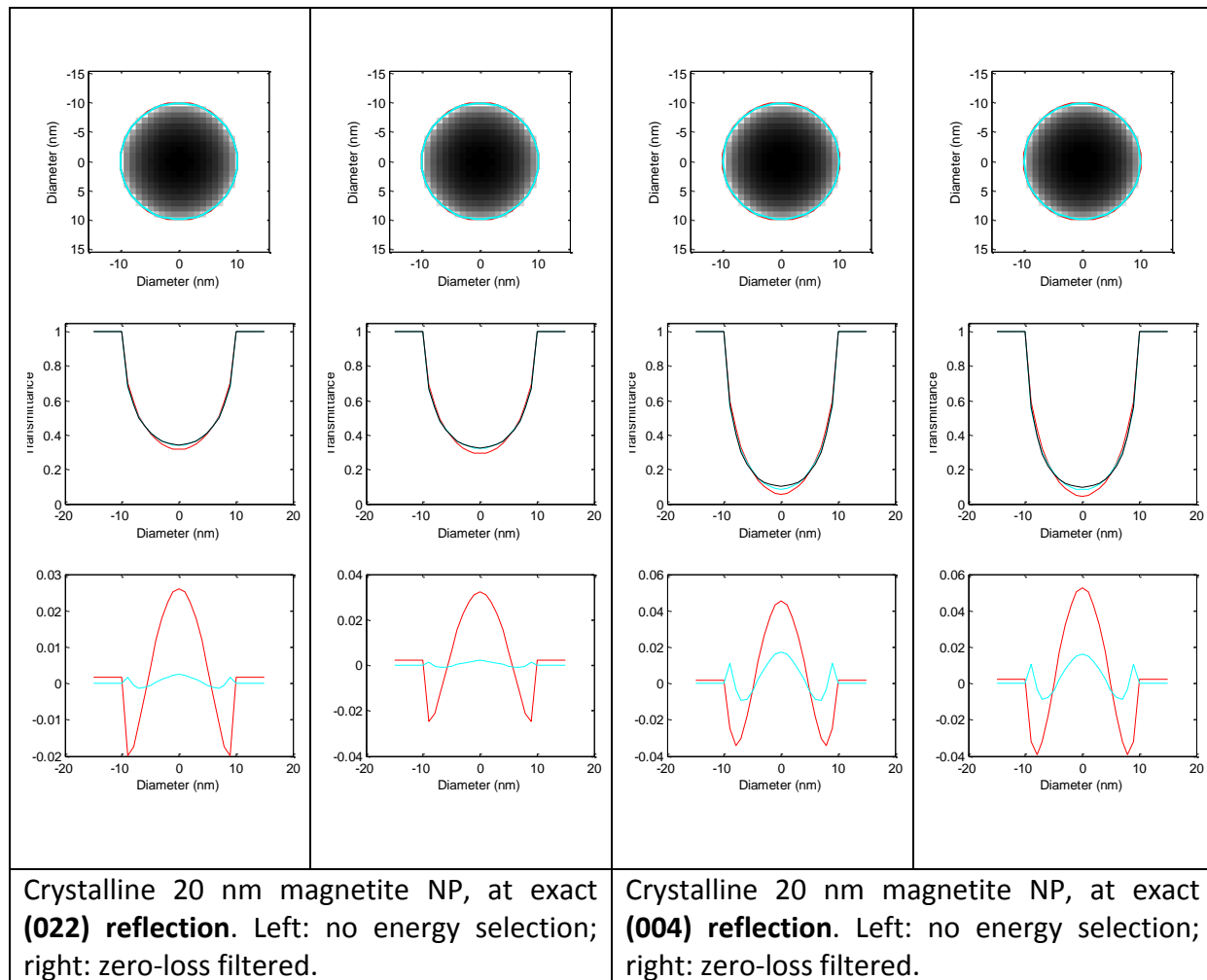
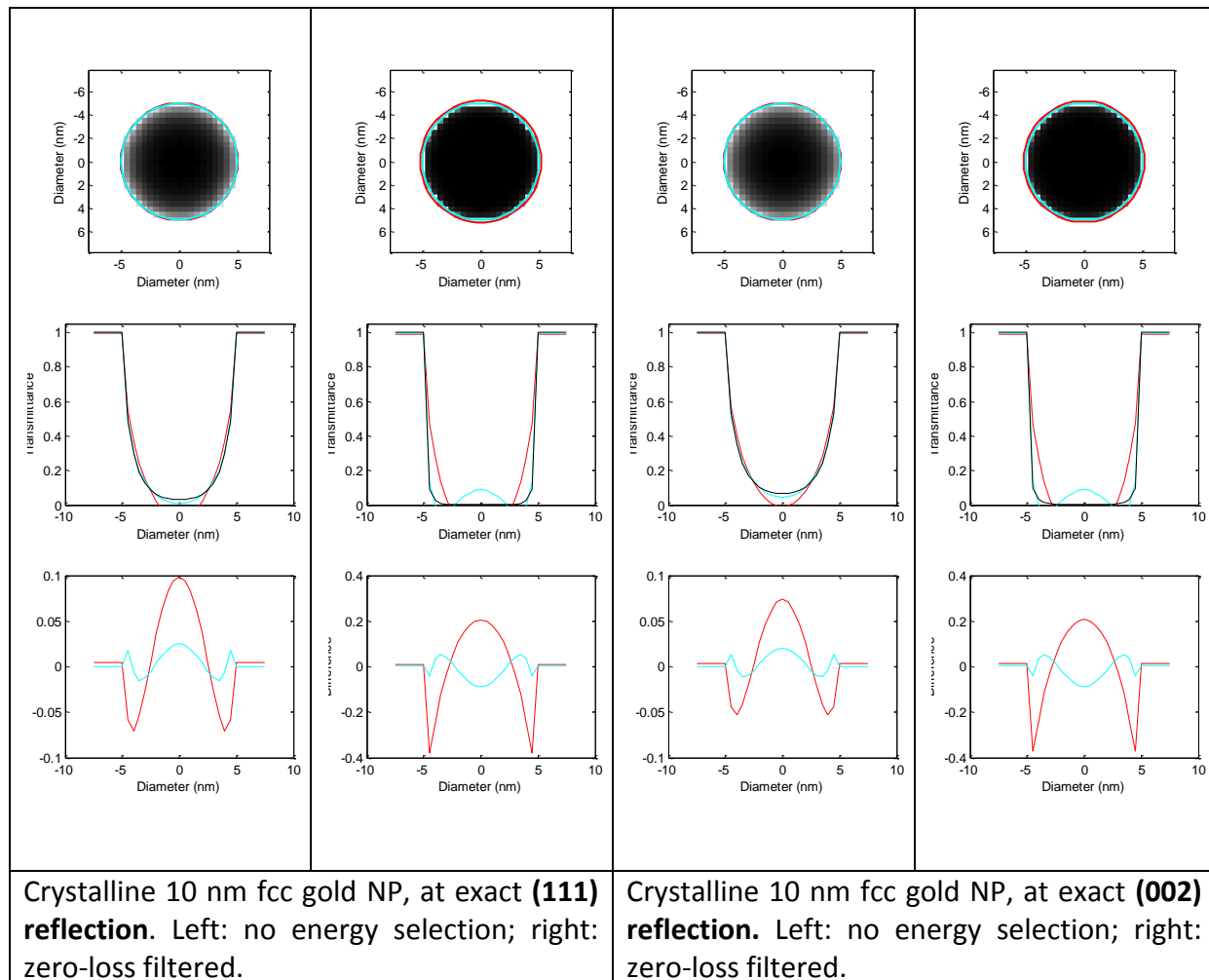


Figure S3. Results of fitting a linear $J = j_0 + j_1 t$ or quadratic $J = j_0 + j_1 t + j_2 t^2$ model to reference images of crystalline 20 nm magnetite (Fe_3O_4) and 10 nm fcc gold (Au) spherical NPs computed by general theory including elastic and inelastic incoherent scattering, using electrons accelerated to $E_0 = 200$ keV and an objective lens aperture with collection angle $\beta = 5$ mrad. In all reference images the NP is exactly at the diffraction orientation ($s = 0$) for several strong reflections. Images either with or without zero-loss-filtering are shown. Black lines: reference image; red lines: linear model; cyan lines: quadratic model. Top row: grayscale view of the simulated image with edges of the fitted NPs; comparison of the reference and fitted NP profiles; bottom row: difference between reference and fitted profiles.







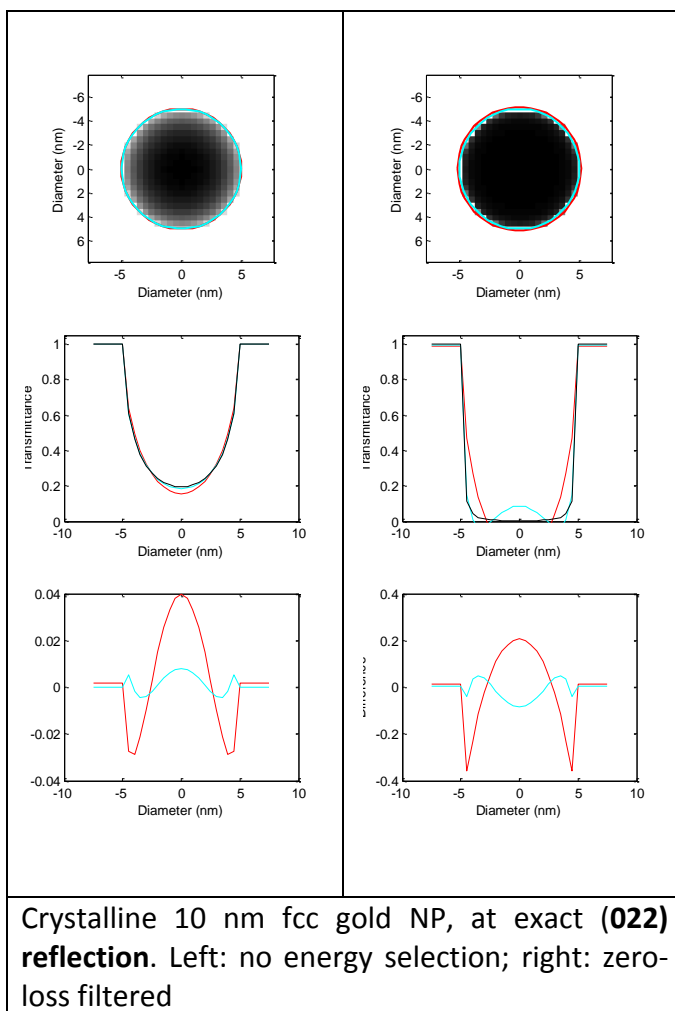
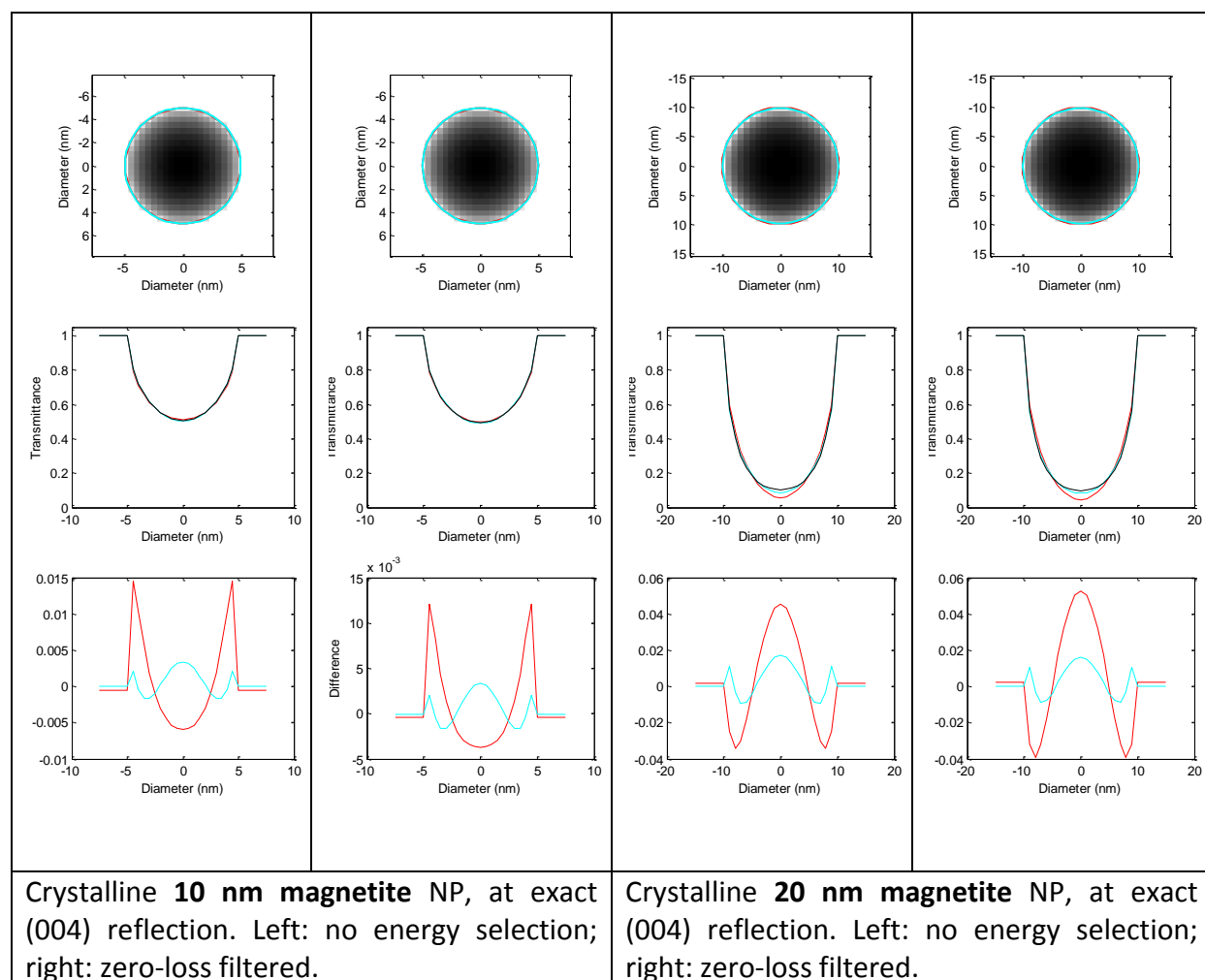
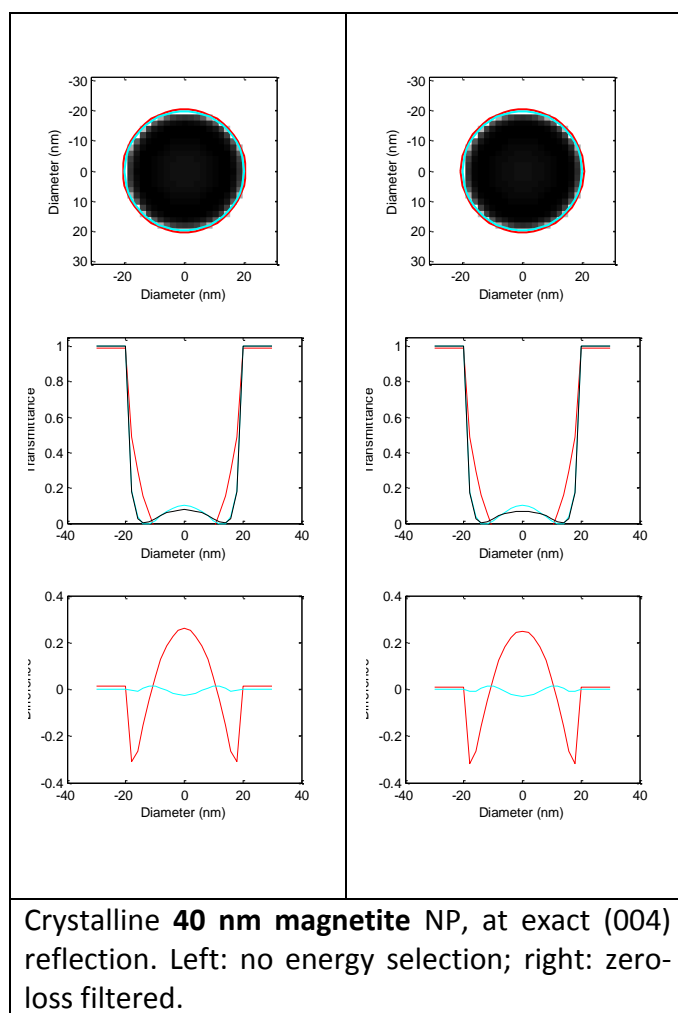
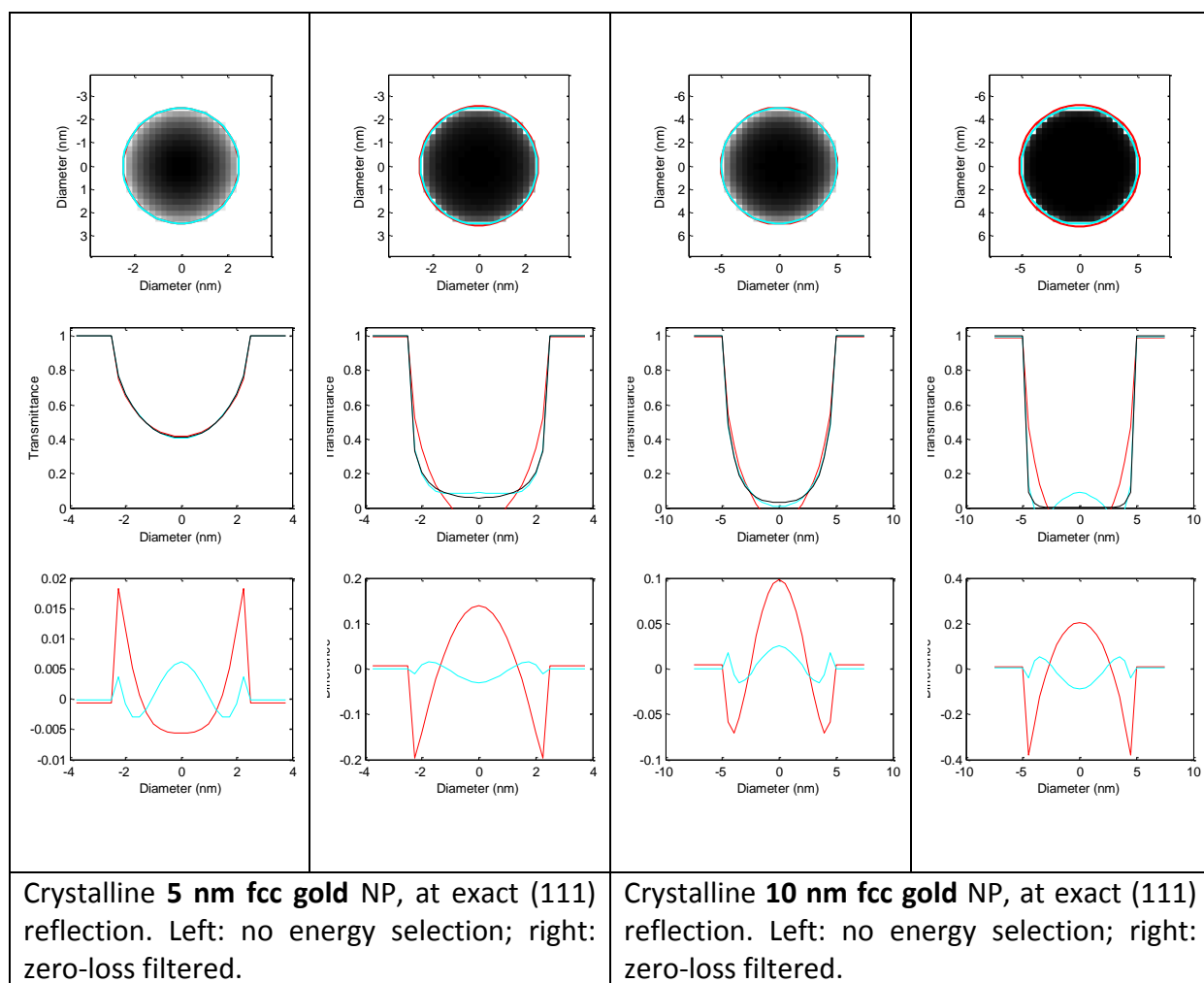


Figure S4. Results of fitting a linear $J = j_0 + j_1 t$ or quadratic $J = j_0 + j_1 t + j_2 t^2$ model to reference images of crystalline magnetite (Fe_3O_4) and fcc gold (Au) spherical NPs computed by general theory including elastic and inelastic incoherent scattering, using electrons accelerated to $E_0 = 200$ keV and an objective lens aperture with collection angle $\beta = 5$ mrad. In all reference images the NP is exactly orientated ($s = 0$) for diffraction at $\mathbf{g} = (004)$ (magnetite) and (111) (gold). Images either with or without zero-loss-filtering are shown. Black lines: reference image; red lines: linear model; cyan lines: quadratic model. Top row: gray-scale view of the simulated image with edges of the fitted NPs; comparison of the reference and fitted NP profiles; bottom row: difference between reference and fitted profiles.







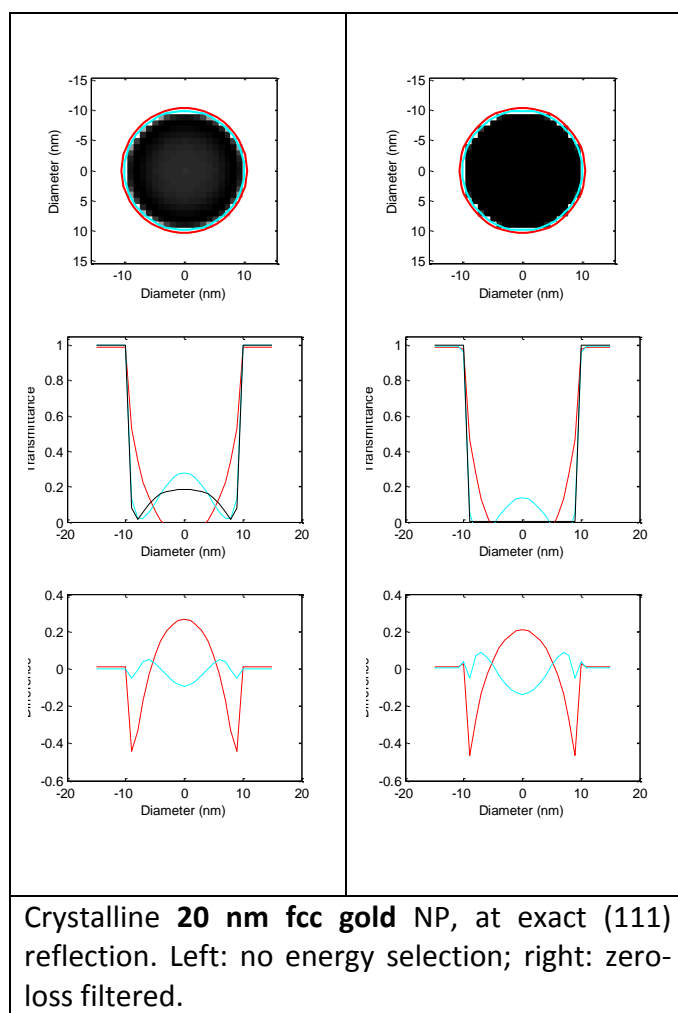
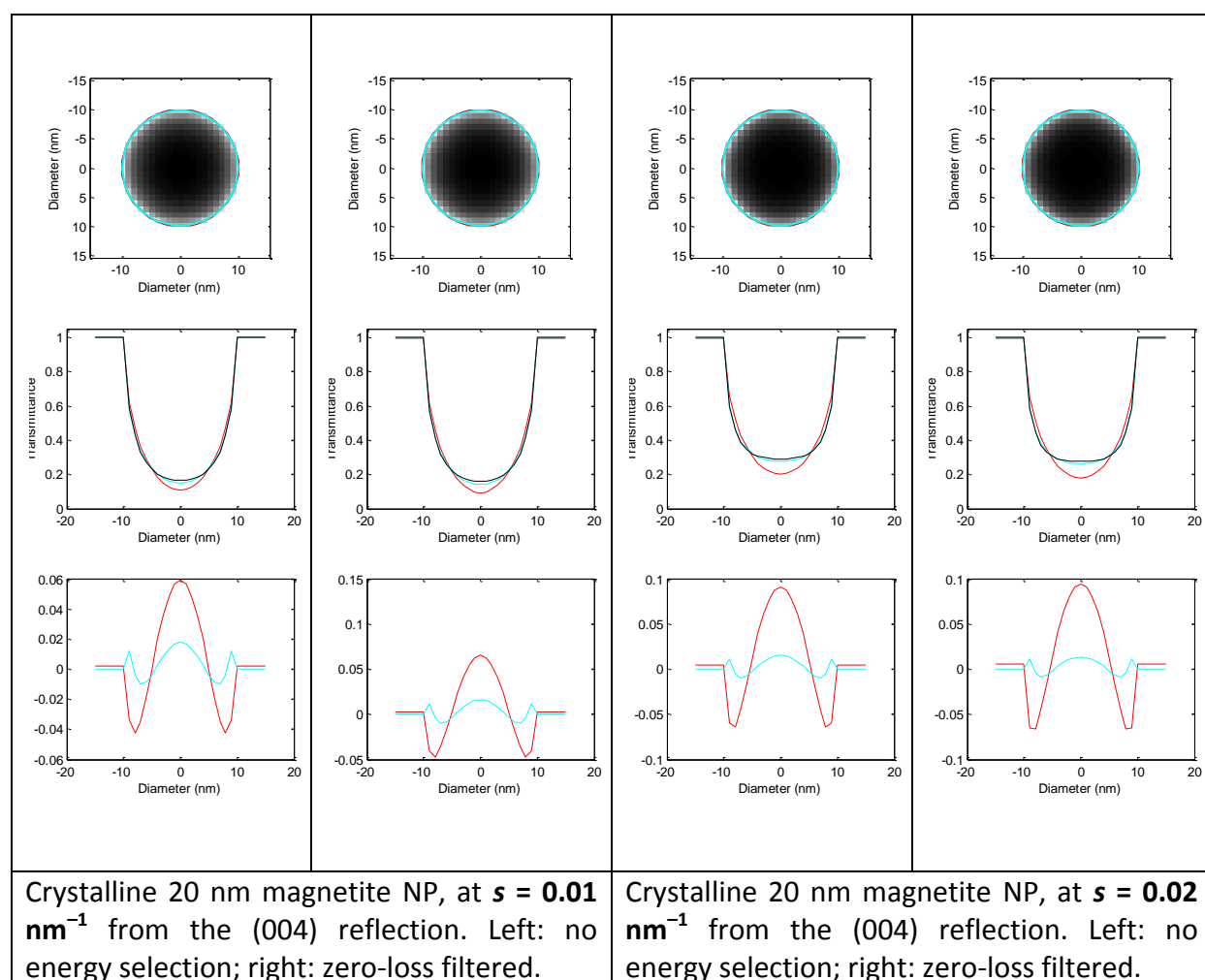
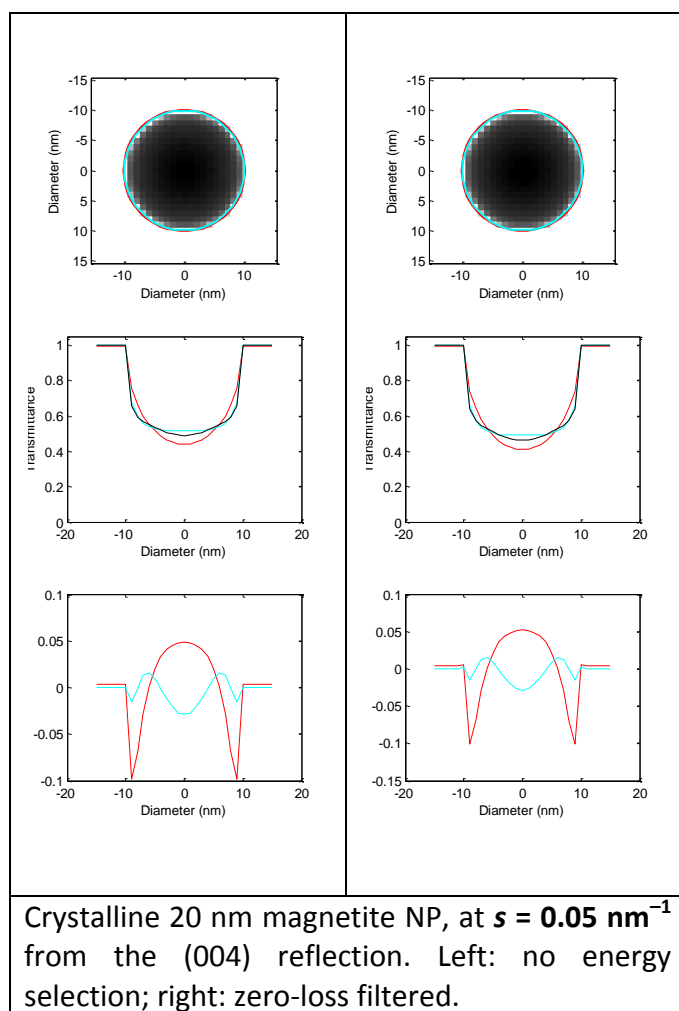
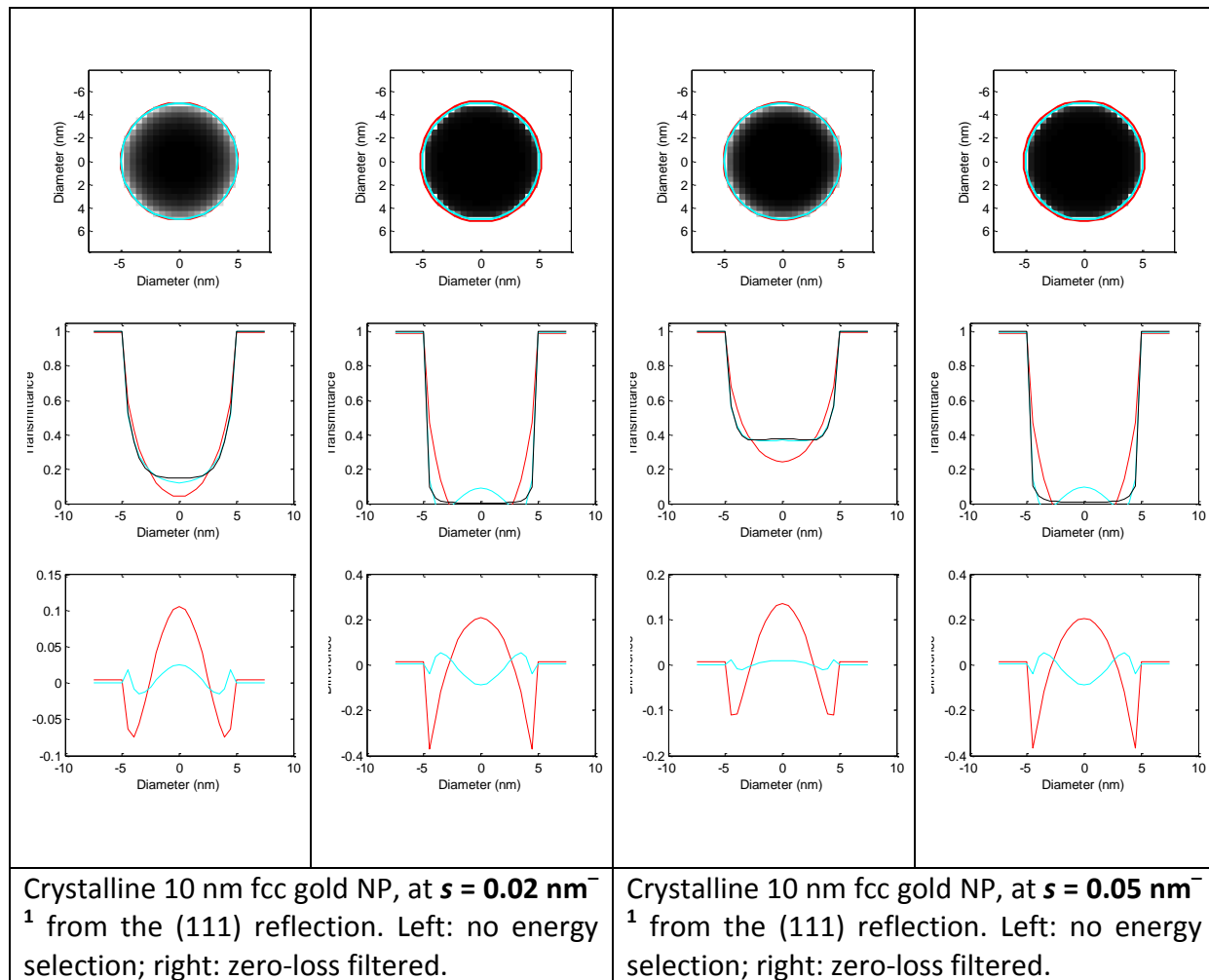


Figure S5. Results of fitting a linear $J = j_0 + j_1t$ or quadratic $J = j_0 + j_1t + j_2t^2$ model to reference images of crystalline 20 nm magnetite (Fe_3O_4) and 10 nm fcc gold (Au) spherical NPs computed by general theory including elastic and inelastic incoherent scattering, using electrons accelerated to $E_0 = 200$ keV and an objective lens aperture with collection angle $\beta = 5$ mrad. The NP has different excitation error s from diffraction condition of $\mathbf{g} = (004)$ (magnetite) and (111) (gold). Images either with or without zero-loss-filtering are shown. Black lines: reference image; red lines: linear model; cyan lines: quadratic model. Top row: gray-scale view of the simulated image with edges of the fitted NPs; comparison of the reference and fitted NP profiles; bottom row: difference between reference and fitted profiles.







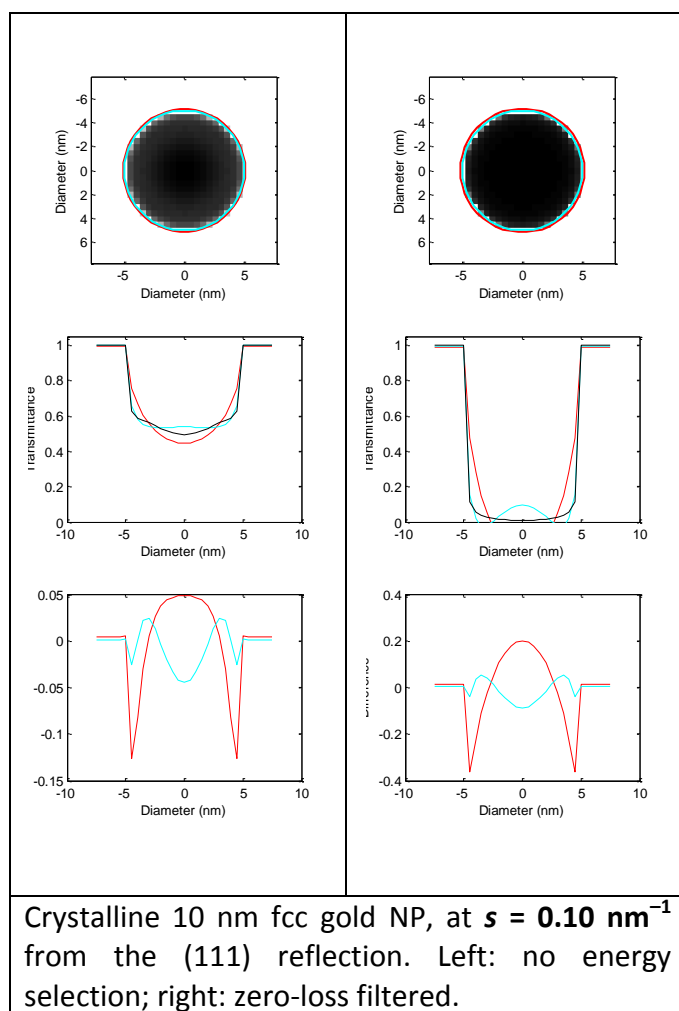
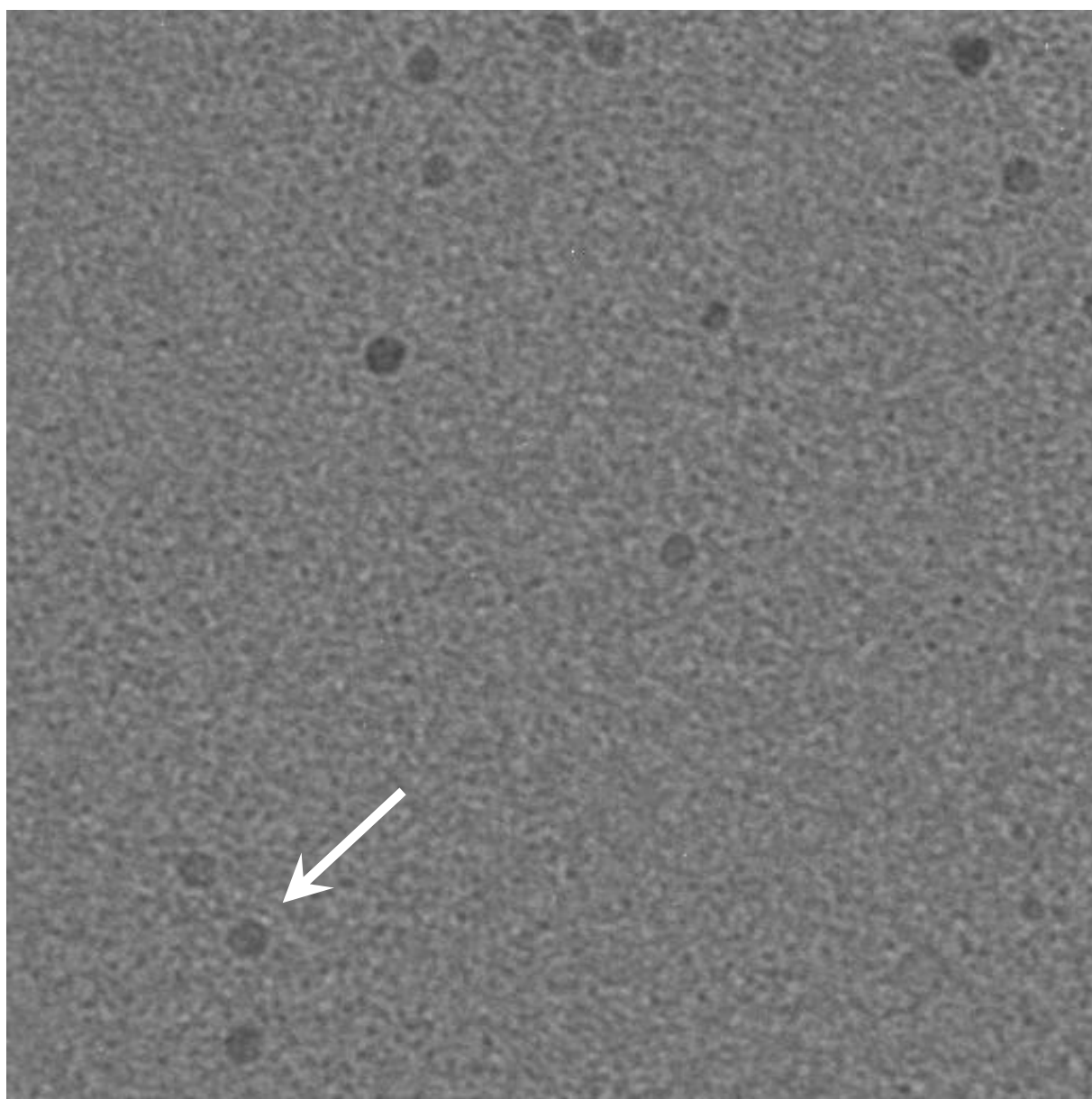
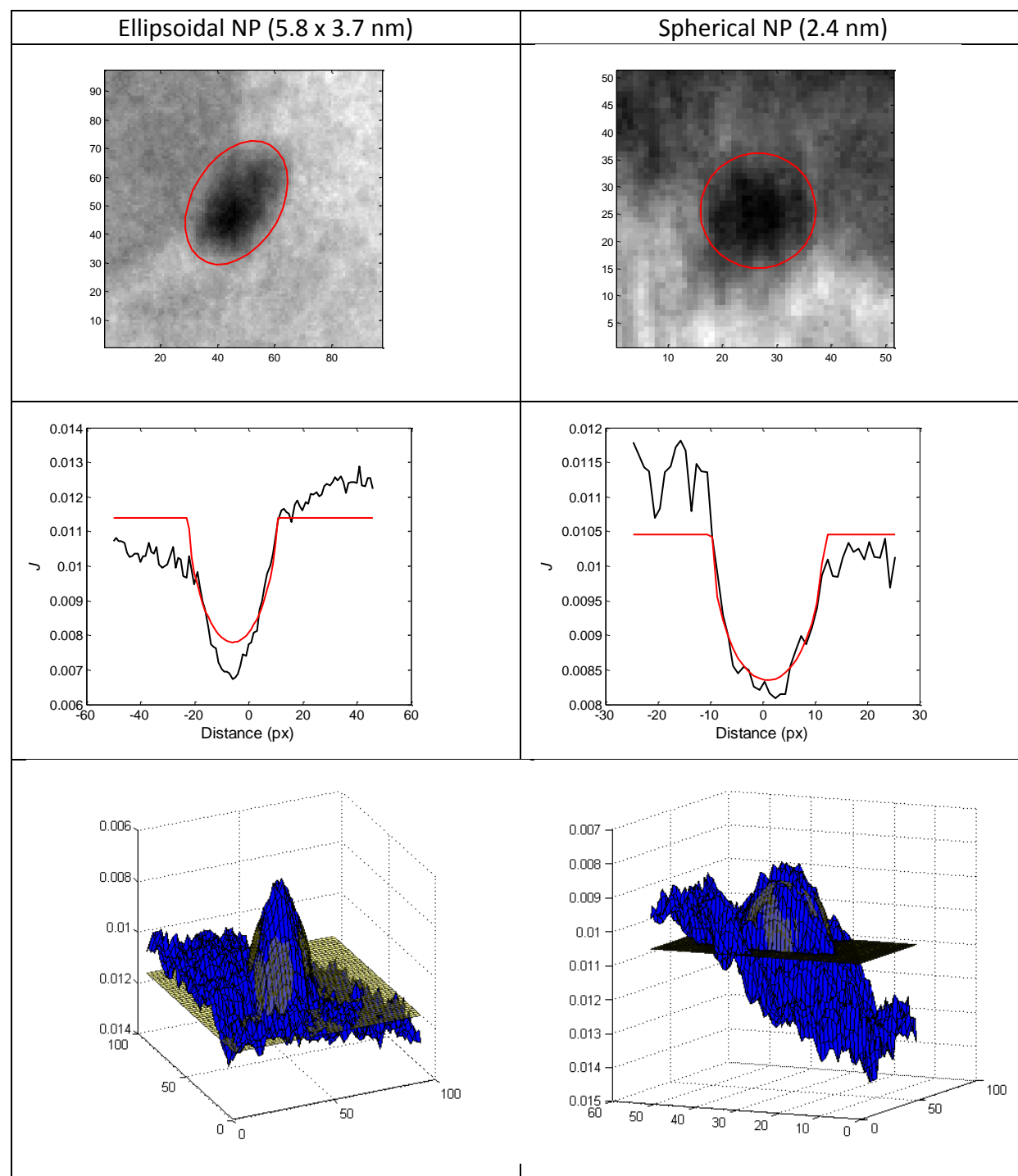


Figure S6. TEM micrograph of monodisperse 9 nm crystalline magnetite nanoparticles with high transmittance and low contrast. The NP fitted in the *Accuracy and Speed in Fitting Experimental Images* Section of the main text is indicated by an arrow. Image size: 278 x 278 nm.



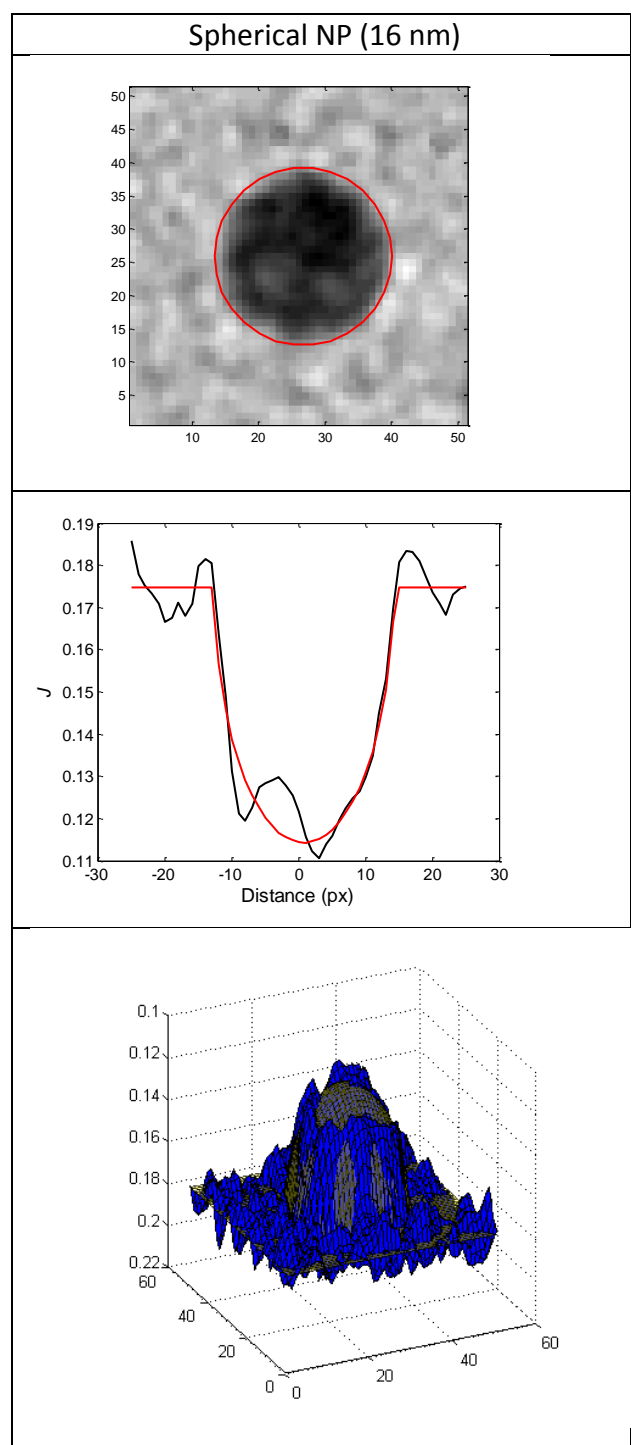
Fitting supported NPs

Figure S7. Results of fitting small platinum metal NPs supported on titania. Top: NP image and best-fit model edge (red). Bottom: experimental (blue) and best-fit image intensity (transparent yellow) surfaces, displayed upside down for the sake of clarity; the vertical axis represents image intensity J normalized to the (0,1) interval. Middle: section through the experimental (black) and best-fit (red) surfaces showing the image intensity profile. Note the sloping background under the spherical NP (right).



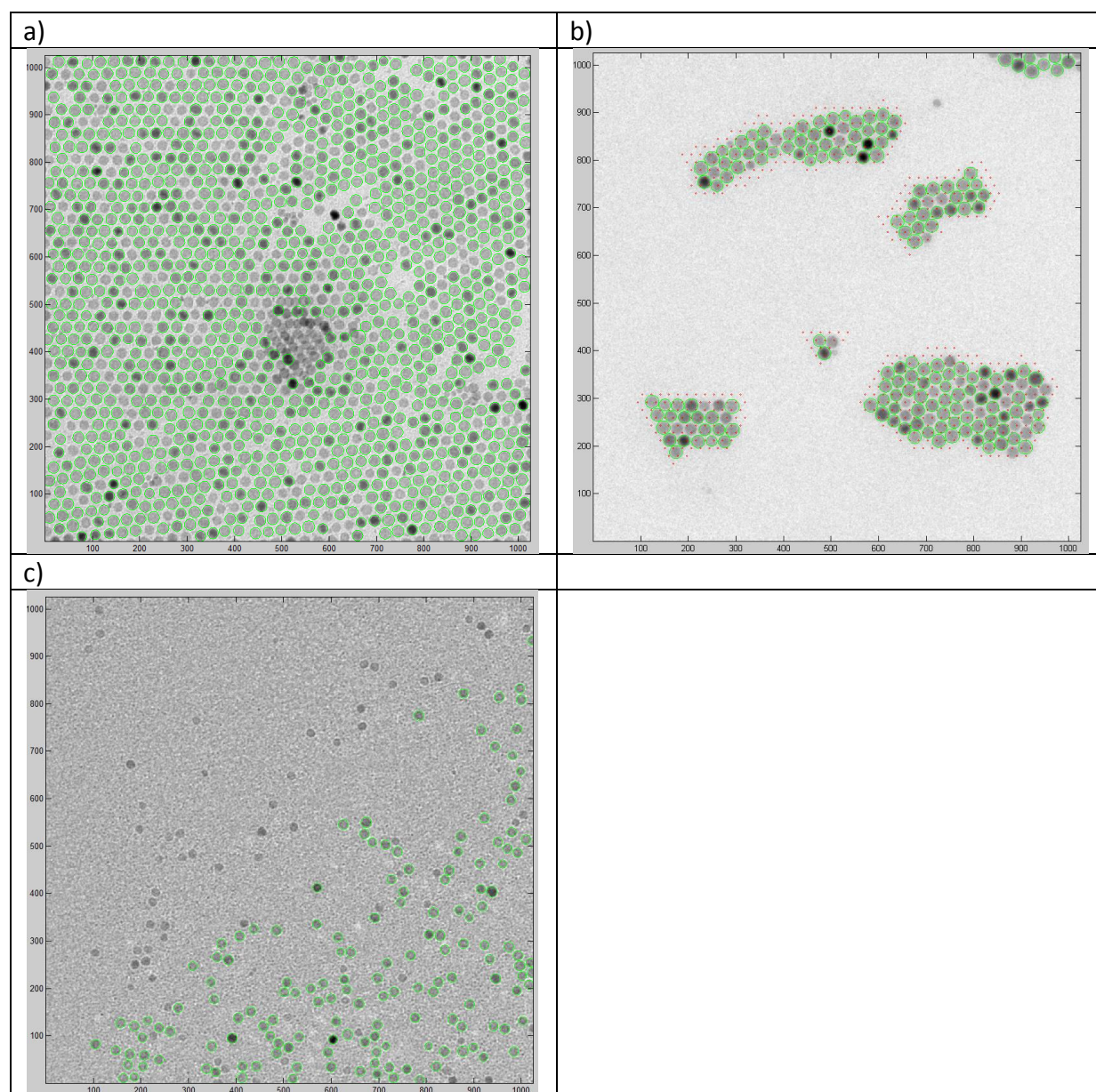
Fitting inhomogeneous NPs

Figure S8. Results of fitting inhomogeneous Cu/Cu₂O/CuO NPs resulting from incomplete oxidation of Cu NPs. [Molteni, G.; Bianchi, C. L.; Marinoni, G.; Santo N.; Ponti, A., *New J. Chem.*, **2006**, *30*, 1137-1139]. Top: NP image and best-fit model edge (red). Bottom: experimental (blue) and best-fit image intensity (transparent yellow) surfaces. Middle: section through the experimental (black) and best-fit (red) surfaces showing the image intensity profile.



Fitting TEM micrographs in automatic mode with $S_{\text{guess}} = 0.75 D_{\text{guess}}$.

Figure S9. Results of fitting TEM micrographs in automatic mode with $S_{\text{guess}} = 0.75 D_{\text{guess}}$. (a) 14 nm spherical MnO NPs; (b) 16 nm spherical Fe_3O_4 NPs (red dots represent the guess centers); (c) 9 nm spherical Fe_3O_4 NPs. The best-fit NP models are shown as green circles. Image size: (a,b) 615 x 615 nm, (c) 470 x 470 nm.



Dependence of the fitting procedure throughput and completeness on the spacing S_{guess} of the guess center grid.

To get further insight into the strong dependence of the procedure throughput and completeness on the chosen S_{guess} , a TEM micrograph of 14 nm spherical MnO NPs (see Figure S9a) has been processed with $S_{\text{guess}}/D_{\text{guess}}$ ranging from 0.375 to 1. The results are shown in Figure S10.

Since the micrograph is filled with NP images, we obtained one valid NP out of three guesses irrespective of the spacing and the time/guess NP and time/valid NP curves are almost parallel. At small S_{guess} , the final NP/valid NP ratio is low since each NP image is fitted several times and redundant NP models are present. Therefore, the time/final NP curve quickly rises at small S_{guess} , leading to a lower effective throughput. Such speed decrease is however accompanied by a more complete recognition of the NP images which approaches 100%. When S_{guess} is close to D_{guess} the throughput is much better but as low as 50% on the NPs present in the micrograph are recognized.

Figure S10. Number of NP models and timings (Windows PC, CPU Intel Core2 Duo E8400 3.0 GHz, 3 GB RAM) from fitting a micrograph of 14 nm MnO NPs with $S_{\text{guess}}/D_{\text{guess}}$ ranging from 0.375 to 1. Top: valid/guess NP ratio (blue), final/valid NP ratio (red), and fraction of NP images which have been fitted (green). Bottom: average time per guess (blue), valid (red) and final (green) NP best-fit model.

